Single-cell CD8+ dynamics in PLWH uncover the depletion of TIGIT+ memory HIV-1-specific cells during long-term ART

Oscar Blanch-Lombarte[1,2], Dan Ouchi[1], Esther Jiménez-Moyano[1], Julieta Carabelli[1,3], Miguel Angel Marin[1], Ruth Peña[1], Adam Pelletier[4], Aarthi Talla[4], Ashish Sharma[4], Judith Dalmau[1], José Ramón Santos[5,6], Rafik-Pierre Sékaly[4], Bonaventura Clotet[1,3,5,6,7] and Julia G. Prado[1,3,8*]

1. IrsiCaixa AIDS Research Institute, Badalona, Barcelona, Spain
2. Universitat Autònoma de Barcelona, Cerdanyola del Vallès, Barcelona, Spain
3. Germans Trias i Pujol Research Institute (IGTP), Badalona, Spain.
4. Pathology Department, Case Western Reserve University, Cleveland, OH, United States.
5. Lluita contra la SIDA Foundation, Hospital Universitari Germans Trias i Pujol, Badalona, Spain
6. Infectious Diseases Department, Hospital Universitari Germans Trias i Pujol, Badalona, Spain
7. Faculty of Medicine, University of Vic - Central University of Catalonia (UVic-UCC), Vic, Spain
8. CIBER Enfermedades Infecciosas (CIBERINFEC), Instituto de Salud Carlos III, Madrid, Spain

*Corresponding author: Julia G. Prado (jgarciaprado@irsicaixa.es). IrsiCaixa AIDS Research Institute, Germans Trias i Pujol Research Institute (IGTP), Crta. Canyet s/n; 08916, Badalona, Barcelona, Spain. Tel: +34 934 656 374.

Abstract

The expression of inhibitory receptors (IRs) is a hallmark of CD8+ T-cell exhaustion (Tex) in people living with HIV-1 (PLWH). Understanding the dynamics of IRs expression in PLWH on long-term antiretroviral treatment (ART) is critical to overcoming CD8+ Tex and designing broadly applicable HIV-1 immunotherapies for cure. To address this, we combine high-dimensional immunophenotype and unsupervised single-cell analysis of IRs and functional markers in CD8+ T-cells among 24 PLWH over a decade of ART. We found irreversible alterations of IRs co-expression patterns in CD8+ T cells and identified negative associations between the frequency of TIGIT+ and TIGIT+TIM-3+ and immune status. Moreover, the single-cell dynamics of total, polyclonal, and HIV-1-specific CD8+ T-cells delineate a complex reshaping of memory-like and effector-like cellular clusters during long-term ART. Indeed, HIV-1 specific-CD8+ T-cells dynamics uncover the selective reduction of memory-like cellular clusters sharing TIGIT expression and low CD107a. Ex vivo single TIGIT but not combinatorial TIGIT+TIM3 antibody blockade restored CD107a expression in HIV-1-specific CD8+ T cells, particularly within the memory compartment. Collectively, these results profile single-cell dynamics of IRs expression across the CD8+ T-cell landscape and propose TIGIT as a target for precision immunotherapies in PLWH on long-term ART.

Introduction

The ART introduction has been the most successful strategy to control viral replication, transforming HIV-1 into a chronic condition. However, ART does not cure the infection, and treatment is required lifelong due to a stable viral reservoir, raising the need to find a cure for people living with HIV-1 (PLWH). A sterilizing or functional cure aims to eliminate or control HIV-1 in the absence of ART. In both scenarios, HIV-1-specific CD8+ T cells are likely to play an essential role as they have been widely recognized as a critical factor in the natural control of viral replication (1–5). Proliferative capacity, polyfunctionality, and ex vivo antiviral potency are features of HIV-1-specific CD8+ T cells associated with spontaneous viral control (6–9).

Although ART in PLWH normalizes the levels of CD8+ T cells, potentially preserving the functional characteristics (9–12). Residual viral replication and continuous antigen exposure at the reservoir sites lead to long-term CD8+ T-cell dysfunction and exhaustion (Tex), a critical barrier for HIV-1 curative interventions (13–15). CD8+ Tex is defined by the progressive loss of immune effector functions linked to transcriptional, epigenetic, metabolic changes and the persistent expression of inhibitory receptors (IRs) (16–19).

In HIV-1 infection, the expression of IRs is a hallmark of CD8+ Tex as IRs are continuously expressed despite long-term suppressive ART (20–26). Moreover, IRs expression levels have been associated with disease progression and immune status in PLWH (25,27–32).

Due to multiple pieces of evidence, the interest in evaluating the blocking of IRs or immune checkpoint blockade (ICB) as a therapeutic strategy to reverse CD8+ Tex continuously increases (26,27). Over the last years, several studies support the recovery of proliferative capacity, cell survival, and cytokine production of HIV-1-specific CD8+ T cells through ICB (33,34), and the blockade of the PD-1/PDL-1 axis has been extensively studied, demonstrating the functional recovery of HIV-1-specific CD8+ T cells in PLWH (26,27). Moreover, alternative pathways to PD-1/ PDL-1, including LAG-3, TIGIT, and TIM-3, have been explored as candidates for ICB therapies for HIV-1 infection (33,35–37). Recent data support the combinatorial use of ICB to favor synergistic effects on the recovery of HIV-1-specific CD4+ and CD8+ T-cell function (38,39).

The unprecedented success of the clinical use of ICB in the cancer field (40,41) has prompted the clinical evaluation of ICB in PLWH (42) to boost immunity to reduce or eliminate the viral reservoir. However, the clinical data on the impact of ICB on HIV-1 cure interventions remains unclear (34,43–47). In this context, understanding the functional regulation of CD8+ Tex through the dynamics of IRs expression remains elusive in PLWH on ART. However, it will be critical for target identification to develop widely applicable and precise immunotherapies for HIV-1 cure (48).

For this purpose, we performed a multidimensional comparative, supervised, and unsupervised single-cell analyses of IRs, including PD-1, TIGIT, LAG-3, TIM-3, CD39, and functional markers across the landscape of CD8+ T cells in PLWH over a decade of ART, PLWH with early infection and healthy controls. We characterize with high-resolution the dynamics of CD8+ T cells, and single-cell analyses unfold a

selective decrease of memory-like cellular clusters sharing TIGIT expression and low CD107a expression in the dynamics of HIV-1-specific CD8+ T-cell recovered by TIGIT blockade. These results provide evidence for the continuous reshaping of IRs expression in CD8+ T-cells at three levels studied and propose TIGIT as a target for precision immunotherapies in PLWH.

Results

Irreversible alterations in CD8+ T-cell frequencies and IRs expression patterns in PLWH during long-term ART

Although the expression of IRs is a hallmark of CD8+ Tex in HIV-1 infection (20–26), a longitudinal and detailed characterization of the combinatorial expression of IRs across CD8+ T-cell lineages in PLWH on long-term ART is still missing. To do this, we combined the analyses of IRs (PD-1, TIGIT, LAG-3, TIM-3, and CD39) and lineage markers (CD45RA, CCR7, and CD27) in CD8+ T cells in longitudinal samples from PLWH on ART. We compare samples from PLWH on ART in S1 (median of 2.2 years) and S2 (median of 10.1) with samples from PLWH with early infection (Ei) and healthy controls (HC) (**Figure 1A**). The epidemiological and clinical characteristics of the study groups are included in **Supplemental Table 1**.

As shown in **Fig 1B**, we identified alterations in the co-expression patterns of IRs in central memory (CM) and transitional memory (TM) CD8+ T cells in PLWH on ART compared with HC. These perturbations were maintained in CM but not TM cells in S2 samples (**Figure 1B**). After deconvolution of IRs co-expression patterns in terms of the number of receptors across CD8+ T-cell lineages, we observed alterations in CM mainly driven by a significant increase of cells expressing one IR and a reduction of cells lacking IRs expression (**Figure 1C**). We confirmed similar findings at the level of total and CD8+ T-cell subsets (**Supplemental Figure 1, A-C**). Moreover, we observed an augment in effector memory (EM), TM, and effector (EFF) CD8+ T cells co-

expressing three or more IRs in Ei and S1 that normalized in S2 when compared to HC (**Figure 1C**). Of note, out of the 32 possible combinations of IRs studied in CD8+ T-cell subsets (**Supplemental Figure 1D**), TIGIT$^+$ expression alone in CM and TM and TIGIT$^+$TIM-3$^+$ co-expression in CM and EFF CD8+ T cells accounted for continuous increases in frequency over a decade of suppressive ART (**Figure 1D**).

These initial findings led us to postulate associations between the expression of IRs in CD8+ T cells, persistent immune activation on ART, and immune recovery measured by CD4+ T-cell counts. For this purpose, we performed correlation analyses that revealed several negative correlations between the frequency of CD8+ T cells expressing IRs alone or combined and CD4+ T-cell counts across study groups (**Figure 1, E-G)**. Focusing in S2 samples (**Figure 1G**), we found significant negative correlations between CD4+ T-cell counts and the frequency of total CD8+ T cells expressing TIGIT$^+$ alone (p=0.0157, r=-0.58), CD8+ T cells expressing 1 IRs (p=0.0386, r=-0.54) or >1 IRs (p=0.0386, r=-0.51). At the level of CD8+ T-cell populations, the expression of 2 IRs in CM and >1 IR in TM CD8+ T cells negatively correlated with CD4+ T-cell counts in S2 (p=0.0072, r=-0.64; p=0.0346, r=-0.52, respectively) (**Figure 1G**). Despite successful long-term ART, these correlations suggest a relationship between IRs expression and immune status in PLWH on ART.

These data support irreversible changes of IRs expression in total CM and TM CD8+ T cells in PLWH on ART. The alterations in co-expression patterns marked by increased CD8+ T-cell populations expressing 1 or >1 IRs, particularly TIGIT$^+$ alone and TIGIT$^+$TIM-3$^+$, uncover associations between IRs expression patterns and immune status in PLWH on ART.

Single-cell dynamics of effector-like and memory-like CD8+ T-cell clusters

Next, to further characterize the dynamics of IRs expression in total CD8+ T cells in PLWH on ART at the single-cell level, we performed an unsupervised single-cell net-SNE analysis. We concatenated 1,988,936 total CD8+ T cells and analyzed the phenotypes with the topographical regions of each surface marker (**Figure 2, A-B**). Cells were classified into 38 cellular clusters distributed according to relative marker expression of 14 parameters and represented using net-SNE and heatmaps (**Figure 2, C-D**). Out of the 38 clusters identified, we observed 15 cellular clusters with statistical differences in frequency between study groups (**Figure 2D**). To increase the number of cells for quantitative statistical assessments between clusters, we merged (#5, #6, and #7), (#9 and #10), and (#12, #13, and #14), accounting for low frequencies of cells with high similitudes (**Figure 2D**). Out of these 15 cellular clusters, #1, #5-7, #8, #9-10, #11, and #12-14 were markedly altered in composition and proportion in Ei vs. HC, and clusters #1 to #15 in HC vs S1, S2 (**Figure 2E**). We observed two patterns of cluster distribution in PLWH on ART; a set of clusters decreased in frequency on ART (#1 to #7, **Figure 2E**) and a set of clusters that augmented in frequency on ART (# 8 to #15, **Figure 2E**). Low differentiated CD8+ T-cell populations characterized clusters #1 to #7 with memory-like phenotypes lacking or with decreased expression of IRs. Concomitant with this contraction, clusters #8 to #15 increased in frequency sharing effector-like phenotypes and co-expression of IRs (**Figure 2E**). Regarding the IRs expression, PD-1 expression was dominant in clusters #1, #2, #3, and #11. By contrast, clusters #8, #9, and #10 are characterized by the co-expression of TIGIT, LAG-3, and TIM-3. Notably, we identified the expansion of a unique cluster #15 with a naïve-like phenotype on ART with TIGIT expression (**Figure 2D-E**).

Collectively, these results identify dynamics of contraction and expansion of CD8+ cellular clusters in PLWH on ART. Indeed, the ART period is characterized by a

continuous increase of effector-like CD8+ T-cell clusters with high heterogeneity and complexity of IRs expression patterns.

Single-cell dynamics of effector-like and memory-like polyclonal TCR-activated CD8+ T cells

Then, we explored the dynamics of IRs expression in polyclonal TCR-activated CD8+ T cells at the single-cell level using unsupervised net-SNE analysis. Polyclonal TCR-activated CD8+ T cells were defined as those cells producing at least one functional marker, including CD107a, IFNγ, or IL-2, under SEB stimulation **(Figure 3, A-B)**. Finally, 253,021 cells were concatenated among groups and identified 29 unique clusters represented by net-SNE and heatmaps (**Figure 3, C-D**). Out of the 29 clusters, 14 clusters showed statistical differences in frequency between study groups (**Figure 3D**). As previously done, to increase the number of cells for quantitative statistical assessments, we merged clusters with high similitudes (#1 and #2), (#4 and #5), and (#8, #9, and #10). Clusters (#1-2), (#4-5), #7, and #14 were significantly altered in proportions in Ei and #1 to #14 clusters on ART (**Figure 3E**). We observed similarities with previous analyses of total CD8+ T cells and characterized dynamics of contraction and expansion at the level of CD8+ T-cell clusters susceptible to TCR activation. Focusing on the alterations in ART (S1 and S2), we observed the contraction of cellular clusters (#3 to #6) in HC vs. ART sharing memory-like phenotypes with various patterns of IRs co-expression (**Figure 3E**). By contrast, clusters (#8 to #13) increased in frequency on S1, and clusters #12 and #13 continuously increased over S2. These two particular clusters shared effector-like features, co-expression of IRs and IFNγ (**Figure 3D**). Across the functional markers, IL-2 was predominantly expressed in #4-5 and #6, and CD107a and IFNγ in clusters #8 to #13. These data support complex dynamics of polyclonal CD8+ cellular clusters susceptible to TCR activation with a continuous

expansion of effector-like clusters with co-expression of IRs, CD107a, and IFNγ in PLWH on ART.

Continuous decrease of HIV-1-specific CD8+ T-cell clusters sharing memory-like phenotype TIGIT expression and low CD107a in PLWH during long-term ART

To characterize the dynamics of IRs expression in HIV-1-specific CD8+ T cells at the level of single-cell immunophenotype in PLWH on ART. We analysed 53,751 cells concatenated based on the production of at least one cytokine (CD107a, IFNγ, or IL-2) in response to HIV-1-Gag antigens using a similar unsupervised net-SNE analysis (**Figure 4, A-B**). The high-dimensional mapping defined 26 cellular HIV-1-specific clusters, five clusters with significant differences between Ei and ART groups (S1 and S2) (**Figure 4, C-D**). In contrast to previous results, four out of five clusters decreased in frequency (#1 to #4, both in S1 and S2) on ART (**Figure 4E**). Only cluster #5 with a memory-like phenotype and expression of three cytokines, showed a different trend from the rest increasing on ART. Phenotypically, clusters #1, #2, and #3 shared a memory-like phenotype. Of note, #1 and #2 showed higher co-expression of IRs, mainly PD-1 and TIGIT, in the absence of functional markers CD107a and IFNγ (**Figure 4D**). Cluster #4 with effector-like phenotype shared with #1 and #2 but lacked CD107a. Meanwhile, cluster #3 with co-expression of IRs (TIGIT, PD-1, and TIM-3) had a more functional profile (**Figure 4D**). Although CD107a, IFNγ, and IL-2 profiles differed between clusters #1 to #4, they shared common phenotypic characteristics, including TIGIT expression and, less frequently, TIM-3 expression.

These findings led us to postulate the predominant role of $TIGIT^{+}$ and potentially $TIGIT^{+}TIM\text{-}3^{+}$ co-expression as possible signatures of CD8+ Tex. To further validate these findings using unsupervised and supervised data analyses, we backgated CD107a,

IFNγ, and IL-2 producing cells in responses to HIV-1 into the CM specific-CD8+ T cells expressing TIGIT^{+} and TIGIT^{+}TIM-3^{+}. As shown in **Figure 4F**, we confirmed alterations in the functionality of TIGIT^{+} CM HIV-1-specific CD8+ T cells. We identified CD107a as the functional marker affected in CM HIV-1-specific CD8+ T cells in PLWH on ART (**Figure 4F**). No changes were observed in TIGIT^{+}TIM-3^{+} cells (data not shown).

Thus, the single-cell dynamics of HIV-1-specific CD8+ T cells suggest a selective decrease of memory-like clusters with shared TIGIT expression and low CD107a during long-term ART.

Ex vivo TIGIT but not TIGIT+TIM-3 pathway blockade restores CD107a expression in HIV-1-specific CD8+ T cells

Given the possible association between TIGIT^{+} expression in HIV-1-specific CD8+ T cells in PLWH on ART and loss of CD107a, we decided to explore the blockade of TIGIT and TIM-3 pathways as an immunotherapeutic target for the recovery of CD107a and potentially IFNγ, and IL-2 production. We performed short-term ICB experiments with antibodies αTIGIT alone or combined with αTIM-3 in PBCMs from S1 and S2 samples. After ICB, we monitored changes in CD107, IFNγ, and IL-2 in total HIV-1-specific CD8+ T-cell and subsets. Net-SNE projections in **Figure 5A** represent the markers studied. Short-term ICB experiments demonstrate an increase of CD107a expression in HIV-1-specific CD8+ T-cells in the presence of αTIGIT (isotype vs. αTIGIT; $p<0.05$) and αTIGIT + αTIM-3 (isotype vs. αTIGIT + αTIM-3; $p<0.05$) (**Figure 5B**). Moreover, the increase in CD107a expression upon αTIGIT was consistent across HIV-1-specific CD8+ T-cell subsets and particularly marked for CM CD8+ T cells (isotype vs. αTIGIT; in CM $p<0.005$) (**Figure 5C**). Of note, dual

blockade of αTIM-3 and αTIGIT did not show any additive effect but rather a detrimental effect in HIV-1-specific CD8+ T-cell subsets except for TM (isotype vs. αTIGIT + αTIM-3; $p<0.05$) (**Figure 5D**). No changes in IFNγ and IL-2 production were observed (**Figure 5, B-D**). These results support the specific targeting of TIGIT to recover the degranulation capacity in HIV-1-specific CD8+ T cells, particularly within the CM subset.

Discussion

CD8+ Tex displays a range of functional defects in PLWH early in HIV-1 infection and on ART (16–19). The expression of IRs is a hallmark of Tex (20,22,23) (14), and co-expression of IRs has been associated with HIV-1 disease progression (15,25,29,30,32) and cancer severity (49–51). ICB has demonstrated promising results in the cancer field (40,41), but the use of ICB as an HIV-1 cure intervention remains unclear (34,43–47). Understanding the dynamics of IRs expression in the context of CD8+ T-cell function in PLWH on ART is essential to guide target identification in developing widely applicable and precise HIV-1 cure immunotherapies based on ICB (48).

Here, we combined supervised and unsupervised single-cell analysis to delineate with unprecedented resolution the dynamics of IRs expression at three levels across the landscape of CD8+ T cells in PLWH over a decade on ART. In this way, our design overcomes limitations of previous cross-sectional studies and analysis of single IRs (20,23,25,29,32). In agreement with previous studies, our data reported a marked and continuous increase of TIGIT expression in memory CD8+ T cells in PLWH on ART (25), (24). Specifically, TIGIT^{+} expression alone increased in CM and TM, and TIGIT^{+}TIM-3^{+} expression increased in CM and EFF CD8+ T cells in PLWH on ART. Moreover, we identify negative associations between TIGIT expression in CD8+ T cells and immune recovery expressed as CD4+ T-cell levels in PLWH over a decade on ART. These continuous increase in the expression of TIGIT^{+} or TIGIT^{+}TIM-3^{+} may directly reflect ongoing immune activation despite fully-suppressive ART (24,25,30,50,52). These data support a potential us of TIGIT expression in CD8+ T cells as a biomarker of immune activation in PLWH on ART.

The implementation of single-cell immunophenotypic analyses of CD8+ T-cells confirmed the presence of heterogeneous IRs co-expression patterns, adding complexity to previous studies (16,21,30,53,54). In addition, single-cell immunophenotyping delineated previously unreported dynamics of contraction and expansion across CD8+ T-cellular clusters and study groups. In PLWH on ART, these dynamics were characterized by contraction of memory-like CD8+ cellular clusters lacking or with decreased expression of IRs and continuous increase of effector-like CD8+ clusters with high heterogeneity and complexity of IRs expression patterns. In this sense, we delineated how IRs co-expressions emerge in PLWH during early HIV-1 infection and persist despite over a decade of suppressive ART. These findings suggest that the expansions of effector-like CD8+ T cells with IRs co-expressions become irreversible and fixed in PLWH on ART. In this line, previous studies support irreversible epigenetic scars of HCV-specific and exhausted CD8+ T cells after HCV cure (55).

Similarly, CD8+ T cells susceptible to polyclonal TCR-activation revealed a continuous reshaping of effector-like and memory-like cellular clusters. While polyclonal memory-like clusters with IRs co-expression showed a contraction, polyclonal effector-like clusters co-expressing IRs increased in frequency in PLWH on ART. These data may indicate a link between IRs co-expression and the functional status of polyclonal TCR-activated CD8+ T cells. Therefore, IRs co-expression may be involved in Tex but also potentially to T-cell activation through the cellular reshaping of memory and effector-like clusters. In addition, the continuous increased in frequency of effector-like cluster suggest both antigen-dependent expansion derived directly from persistence of HIV-1 antigens or indirectly by the exposure to other viral antigens.

Single-cell immune profile of HIV-1-specific CD8+ T-cell clusters revealed a continuous depletion in the frequency of memory-like cells, sharing TIGIT expression and combinatorial expression of CD107a, IFNγ, and IL-2. Indeed, functional data from single-cell analyses and classical analyses coincided to identify low CD107a expression in $TIGIT^{+}$ central memory HIV-1-specific CD8+ T-cells. These data support the role of TIGIT as a signature of Tex (25). Indeed, the blockade of the TIGIT pathway using monoclonal antibodies restored CD107a expression in a precise and differential manner across cellular compartments of HIV-1 specific CD8+ T-cells and particularly increasing the expression of CD107a in central memory cells. To our knowledge, this is the first study to demonstrated the recovery of CD107a expression in HIV-1-specific CD8+ T cells by TIGIT blockade. The mechanism behind TIGIT signalling blockade and CD107a expression is still unknown but it will be critical to provide insights to restore CD8+ T cells degranulation capacity. Low CD107a expression has been linked to the terminal $T\text{-}bet^{dim}Eomes^{hi}$ exhausted phenotype. Although HIV-1-specific CD8+ T cells expressing TIGIT can degranulate to certain extend, most degranulating cells do not express granzyme B losing their cytotoxic capacity (17,24). In contrast to previous data, we did not observe an increase in IFNγ by TIGIT blockade, differences between study groups regarding time on ART should be considered (25). Our findings further support the need to profile PLWH in a personalized and precise manner to identify those individuals that may benefit from immunotherapeutics.

Our study found a detrimental effect in restoring CD107a expression by TIGIT+TIM-3 combinatorial blockade. This observation may relate to the redundancy and promiscuity of the IRs biology. In the case of TIM-3, the receptor engages multiple ligands,

including Gal-9, CEACAM-1, PtdSer, and HMGB-1 (56,57). These data suggest that TIM-3 blockade may not be enough to disrupt interactions with the various ligands. In this context, we cannot exclude the impact of the blockade of TIGIT+TIM-3 pathways in other cell types (50,51,58). Additional experiments targeting TIGIT+TIM-3 including other cell types could provide complementary information.

Our study has some limitations. First, the size of the study groups is limited, and the sampling of peripheral blood may underestimate the contribution of TIGIT expression to CD8+ Tex in tissues. Second, additional transcriptomic, epigenetic, and metabolic studies in addition may contribute to complete immune signatures linked to TIGIT expression in CD8+ Tex.

In summary, our study characterizes highly complex dynamics of IRs expressions across the landscape of total, polyclonal TCR-activated, and HIV-1-specific CD8+ T cells in PLHW during long-term ART. These dynamics identify TIGIT as a target to recover CD107a expression in HIV-1-specific CD8+ T-cells in a subset specific manner. These findings may be particularly relevant in the way to design precision immunotherapies in PLWH for HIV-1 cure.

Methods

Study groups

This retrospective study analyzed clinical data and biological sample availability from 3,000 patients assigned to the HIV-1 clinical unit of the Germans Trias i Pujol University Hospital. We excluded individuals with integrase inhibitors, ART as monotherapy, and treatments with mitochondrial toxicity, including Trizivir, d4T, ddI, AZT and blips over the ART period. We included individuals with cryopreserved PBMCs available in our collection. We identified 24 chronically HIV-1-infected individuals who had been treated mainly with a combination of NNRTI and NRTI for more than ten years with sustained virological suppression (<50 HIV-1-RNA copies/ml) and with longitudinal samples at timepoint 1 (S1, 2.2 (1.8 - 2.8) years undetectable on ART) and at time point 2 (S2, 10.1 (7.4 – 12.9) years undetectable on ART) (**Supplemental Table 1**). For comparative purposes, we included 24 early HIV-1-infected individuals (Ei) defined in a window of 1.3 (0.77 - 17.8) weeks after seroconversion in the absence of ART and 24 healthy controls (HC). The groups were balanced by age to the S2 samples to avoid confounding effects on IR expression.

CD8+ T cell immunophenotype

Cryopreserved PBMCs from the study groups were thawed and rested overnight at 37ºC in a 5% CO_2 incubator. The following day, PBMCs were incubated for six hours at 37ºC in a 5% CO_2 incubator under RPMI complemented medium 10% FBS in the presence of CD28/49d co-stimulatory molecules (1µl/ml, BD), Monensin A (1µl/ml, BD Golgi STOP), and anti-human antibody for CD107a (PE-Cy5, clone H4A3, Thermo Fisher Scientific). PBMCs were left unstimulated, stimulated with SEB for polyclonal TCR-activation (1µg/ml, Sigma-Aldrich), and stimulated with HIV-1-Gag peptide pool

(2μg/peptide/ml, EzBiolab). After six hours of stimulation, cells were rested overnight at 4ºC as previously described (34). The next day, PBMCs were washed with PBS 1X and stained 25 minutes with the Live/Dead probe (APC-Cy7, Thermo Fisher Scientific) at RT to discriminate dead cells. Cells were washed with PBS 1X and surface stained with antibodies for 25 minutes at RT. We used CD3 (A700, clone UCHT1, BD), CD4 (APC-Cy7, clone SK3, BD), CD8 (V500, clone RPA-T8, BD), CD45RA (BV786, clone HI100, BD), CCR7 (PE-CF594, clone 150503, BD), CD27 (BV605, clone L128, BD), TIGIT (PE-Cy7, clone MBSA43, Labclinics SA), PD-1 (BV421, clone EH12.1, BD), LAG-3 (PE, clone T47-530, BD), TIM-3 (A647, clone 7D3, BD) and CD39 (FITC, clone TU66, BD) antibodies. Afterward, cells were washed twice in PBS 1X, fixed, and permeabilized with Fix/Perm kit (A and B solutions, Thermo Fisher Scientific) for intracellular cytokine staining with anti-human antibodies of IFNγ (BV711, clone B27, BD) and IL-2 (BV650, clone MQ1-17H12, BD). Finally, stained cells were washed twice with PBS 1X and fixed in formaldehyde 1%.

TIGIT and TIGIT+TIM-3 immune checkpoint blockade experiments

We selected cryopreserved PBMCs from S1 (n=10) and S2 (n=10). Samples were previously characterized by the expression of TIGIT and TIM-3 on total CD8+ T cells. PBMCs were thawed and rested for four hours at 37ºC in a 5% CO2 incubator. Next, cells were incubated under RPMI complemented medium 10% FBS with 1μl/ml of anti-CD28/CD49d and 1μl/ml of Monensin A overnight at 37ºC in a 5% CO2. PBMCs are divided in the following conditions; 1) unstimulated, 2) SEB (1μg/ml, Sigma-Aldrich) and 3) HIV-1-Gag peptide pool (2μg/peptide/ml) in the absence or presence of αTIGIT and/or αTIM-3, and its respective isotype antibodies. For the single blockade of TIGIT (αTIGIT), we included Ultra-LEAF™ purified anti-human TIGIT antibody (10μg/ml,

clone A15153G, Biolegend) or its control isotype Ultra-LEAF™ purified mouse IgG2a antibody (10μg/ml, MOPC-173, Biolegend). For single TIM-3 blockade (αTIM-3), we used Ultra-LEAF™ purified anti-human TIM-3 antibody (10μg/ml, clone F38-2E2, Biolegend) or its respective isotype Ultra-LEAF™ purified mouse IgG1 antibody (10μg/ml, MOPC-21, Biolegend). Finally, we included αTIGIT+αTIM-3 or their respective IgG2+IgG1 isotypes for a combinational blockade. The next day, PBMCs were surface and intracellularly stained with the panel of antibodies and the methodology described in the section above.

Flow cytometry analysis

Stained PBMCs were acquired on an LSR Fortessa cytometer using FACSDiVa software (BD). Approximately 1,000,000 events of PBMCs were recorded per specimen. Antibody capture beads (BD) were used for single-stain compensation controls. Flow cytometry data were analyzed with FlowJo software v10.6.1, and fluorescence minus one (FMO) was used to set manual gates. We analyzed CD8+ T cells by excluding dump and CD4+ T cells. As previously described, IRs were measured in CD8+ T-cell subsets, including Naïve, central memory, transitional memory, effector memory and effector CD8+ T cells (20,34). For polyclonal TCR-activated and HIV-1-specific CD8+ T-cell cytokine production, we subtracted the background of CD107a, IFNγ, and IL-2 from unstimulated PBMCs.

Single-cell immunophenotype data analysis

The phenotypic and functional characterization of cellular populations was analyzed by using t-Distributed Stochastic Neighbor Embedding (t-SNE) (59) and net-SNE (60) dimensionality reduction algorithms to visualize single-cell distributions in two-

dimensional maps. Briefly, cell intensity was z-normalized, and a randomly selected subset of cells, at least 1,000 cells per sample, was passed through the t-SNE algorithm. The resulting t-SNE dimension was then used to predict the position of all remaining CD8+ T cells acquired per sample from each group using the net-SNE algorithm based on neural networks. For functional analysis, we selected TCR-activated polyclonal and HIV-1-specific CD8+ T cells producing at least CD107a, IFNγ, or IL-2 under SEB or HIV-1 conditions, respectively. In addition, we used the Phenograph clustering method (an unsupervised KNN algorithm designed for high-dimensional single-cell data) to find cell communities (or clusters) using the Louvain method. The identified cell communities were represented in a heatmap with the clusters in the columns and the markers of interest in the rows. The color scale shows the median intensity of each marker on a biexponential scale. For each sample, we calculated quantitative assessments of cellular clusters in the percentage of cells to analyze and compare the distribution between HC, Ei, S1, and S2 groups, similarly to the classical flow cytometry analysis. Clusters with high similitudes in marker expression between groups were merged to increase the number of cells for quantitative statistical assessments.

Statistics

Univariate analysis was conducted using nonparametric methods as follows: Mann-Whitney U test for independent median comparison between groups, signed-rank test for paired median changes over time, permutation test for composition distribution between groups, Kruskal-Wallis test for comparison between more than two groups, and spearman linear correlation coefficient to study the association between continuous variables. All statistical tests were under a significance level of 0.05, and statistics were programmed and performed using the R statistical package (61). Moreover, pattern

distribution and graphical representations of all possible Boolean combinations for IRs co-expression and functional markers were conducted using the data analysis program Pestle v2.0 and SPICE v6.0 software (62). Graph plotting was performed by GraphPad Prism v8.0 software and R packages.

Study Approval

The study was conducted according to the principles expressed in the Declaration of Helsinki (Fortaleza, 2013). The Hospital Germans Trias i Pujol Ethics Committee approved all experimental protocols (PI14-084). For the study, subjects provided their written informed consent for research purposes of biological samples taken from them.

Author contributions

OB-L and JGP conceptualized and designed the experiments. OB-L, EJ-M, and RP developed immunophenotyping and acquiring data. OB-L, MAM, RP, and JC developed short-term antibody blockade experiments. OB-L, DO, MAM, AP, AT, AS, R-PS, and JGP performed bioinfomatic analysis. JD, JRS, BC, and JGP recruited the study participants. OB-L and JGP wrote the manuscript. All authors revised it critically for important intellectual content and have approved the final version submitted for publication.

Acknowledgments

We thank the Flow Cytometry Core Facility from the Germans Trias i Pujol Research Institute (IGTP). This work has been presented at the X and XII Spanish National congress of GeSIDA in 2018 (Madrid, Oral Poster PO-44) and 2021 (Málaga, Oral Poster PO-20). Presented at the Conference on Retroviruses and Opportunistic Infections (CROI), Boston, MA, USA, 2020 (Poster 0302), and also presented in the virtual CROI, Chicago, IL, USA, 2021 (Science Spotlight 01358). This research was supported by National Health Institute Carlos III grant PI17/00164. Julia G. Prado holds a Miguel Servet II contract (CPII15/00014) funded by National Health Institute Carlos III (ISCIII). Oscar Blanch-Lombarte was funded by an AGAUR-FI_B 00582 Ph.D. fellowship from Catalan Government and the European Social Fund. Esther Jiménez-Moyano was funded by Redes Temáticas de Investigación en SIDA (ISCIII RETIC RD16/0025/0041). The funders had no role in study design, data collection, and analysis, the decision to publish or draft of the manuscript.

References

1. Borrow P, Lewicki H, Hahn BH, Shaw GM, Oldstone MB. Virus-specific CD8+ cytotoxic T-lymphocyte activity associated with control of viremia in primary human immunodeficiency virus type 1 infection. J Virol. 1994;68:6103–10.
2. Collins DR, Gaiha GD, Walker BD. CD8+ T cells in HIV control, cure and prevention. Nat Rev Immunol. 2020;20:471–82.
3. Mcbrien JB, Kumar NA, Silvestri G. Mechanisms of CD8+ T cell-mediated suppression of HIV/SIV replication. Eur J Immunol. 2018;48:898–914.
4. Cartwright EK, Spicer L, Smith SA, Lee D, Fast R, Lawson BO, et al. CD8+ lymphocytes are required to maintain virus suppression in SIV-infected macaques treated with short-term antiretroviral therapy. Immunity. 2016;45:656–68.
5. Goulder PJR, Walker BD. HIV and HLA Class I: an evolving relationship. Immunity. 2012;37:426–40.
6. Sáez-Cirión A, Lacabaratz C, Lambotte O, Versmisse P, Urrutia A, Boufassa F, et al. HIV controllers exhibit potent CD8 T cell capacity to suppress HIV infection ex vivo and peculiar cytotoxic T lymphocyte activation phenotype. Proc Natl Acad Sci U S A. 2007 Apr;104(16):6776–81.
7. Migueles SA, Osborne CM, Royce C, Compton AA, Joshi RP, Weeks KA, et al. Lytic Granule Loading of CD8+ T Cells Is Required for HIV-Infected Cell Elimination Associated with Immune Control. Immunity. 2008;29(6):1009–21.
8. Nguyen S, Deleage C, Darko S, Ransier A, Truong DP, Agarwal D, et al. Elite control of HIV is associated with distinct functional and transcriptional signatures in lymphoid tissue CD8+ T cells. Sci Transl Med. 2019;11:eaax4077.
9. Perdomo-Celis F, Taborda NA, Rugeles MT. CD8+ T-cell response to HIV infection in the era of antiretroviral therapy. Front Immunol. 2019;10:1–19.
10. Perdomo-Celis F, Velilla PA, Taborda NA, Rugeles MT. An altered cytotoxic program of CD8 + T-cells in HIV-infected patients despite HAART-induced viral suppression. PLoS One. 2019;14:1–24.
11. Tavenier J, Langkilde A, Haupt TH, Henriksen JH, Jensen FK, Petersen J, et al. Immunosenescence of the CD8+ T cell compartment is associated with HIV-infection, but only weakly reflects age-related processes of adipose tissue, metabolism, and muscle in antiretroviral therapy-treated HIV-infected patients and controls. BMC Immunol. 2015;16:1–14.
12. Serrano-Villar S, Sainz T, Lee SA, Hunt PW, Sinclair E, Shacklett BL, et al. HIV-Infected Individuals with Low CD4/CD8 Ratio despite Effective Antiretroviral Therapy Exhibit Altered T Cell Subsets, Heightened CD8+ T Cell Activation, and Increased Risk of Non-AIDS Morbidity and Mortality. PLoS Pathog. 2014;10:e1004078.
13. Ruiz A, Blanch-Lombarte O, Jimenez-Moyano E, Ouchi D, Mothe B, Peña R, et al. Antigen production after latency reversal and expression of inhibitory receptors in CD8+ T cells limit the killing of HIV-1 reactivated cells. Front Immunol. 2019;10:1–16.
14. Jiang W, He Y, He W, Wu G, Zhou X, Sheng Q, et al. Exhausted CD8+T Cells in the Tumor Immune Microenvironment: New Pathways to Therapy. Front Immunol. 2021;11:1–11.
15. Hoffmann M, Pantazis N, Martin GE, Hickling S, Hurst J, Meyerowitz J, et al. Exhaustion of Activated CD8 T Cells Predicts Disease Progression in Primary HIV-1 Infection. PLoS Pathog. 2016;12(7):1–19.

16. Sekine T, Perez-Potti A, Nguyen S, Gorin JB, Wu VH, Gostick E, et al. TOX is expressed by exhausted and polyfunctional human effector memory CD8+ T cells. Sci Immunol. 2020;5:1–15.
17. Buggert M, Tauriainen J, Yamamoto T, Frederiksen J, Ivarsson MA, Michaëlsson J, et al. T-bet and Eomes Are Differentially Linked to the Exhausted Phenotype of CD8+ T Cells in HIV Infection. PLoS Pathog. 2014;10:1–15.
18. Bengsch B, Johnson AL, Kurachi M, Odorizzi PM, Pauken KE, Attanasio J, et al. Bioenergetic insufficiencies due to metabolic alterations regulated by PD-1 are an early driver of CD8+T cell exhaustion. Immunity. 2016;45:358–73.
19. Sen DR, Kaminski J, Barnitz RA, Kurachi M, Gerdemann U, Yates KB, et al. The epigenetic landscape of T cell exhaustion. Science (80-). 2016;354(6316):1165–9.
20. Breton G, Chomont N, Takata H, Fromentin R, Ahlers J, Filali-Mouhim A, et al. Programmed Death-1 Is a Marker for Abnormal Distribution of Naive/Memory T Cell Subsets in HIV-1 Infection. J Immunol. 2013;191:2194–204.
21. Yamamoto T, Price DA, Casazza JP, Ferrari G, Nason M, Chattopadhyay PK, et al. Surface expression patterns of negative regulatory molecules identify determinants of virus-specific CD8+ T-cell exhaustion in HIV infection. Blood. 2011;117:4805–15.
22. Cockerham LR, Jain V, Sinclair E, Glidden D V., Hartogenesis W, Hatano H, et al. Programmed death-1 expression on CD4+ and CD8+ T cells in treated and untreated HIV disease. Aids. 2014;28(12):1749–58.
23. Rutishauser RL, Hartogensis W, Deguit CD, Krone M, Hoh R, Hecht FM, et al. Early and Delayed Antiretroviral Therapy Results in Comparable Reductions in CD8+ T Cell Exhaustion Marker Expression. AIDS Res Hum Retroviruses. 2017;33:658–67.
24. Tauriainen J, Scharf L, Frederiksen J, Naji A, Ljunggren HG, Sönnerborg A, et al. Perturbed CD8+ T cell TIGIT/CD226/PVR axis despite early initiation of antiretroviral treatment in HIV infected individuals. Sci Rep. 2017;7:1–14.
25. Chew GM, Fujita T, Webb GM, Burwitz BJ, Wu HL, Reed JS, et al. TIGIT Marks Exhausted T Cells, Correlates with Disease Progression, and Serves as a Target for Immune Restoration in HIV and SIV Infection. PLoS Pathog. 2016;12:1–28.
26. Trautmann L, Janbazian L, Chomont N, Said EA, Gimmig S, Bessette B, et al. Upregulation of PD-1 expression on HIV-specific CD8+ T cells leads to reversible immune dysfunction. Nat Med. 2006;12:1198–202.
27. Day CL, Kaufmann DE, Kiepiela P, Brown JA, Moodley ES, Reddy S, et al. PD-1 expression on HIV-specific T cells is associated with T-cell exhaustion and disease progression. Nature. 2006;443:350–4.
28. Graydon CG, Balasko AL, Fowke KR. Roles, function and relevance of LAG3 in HIV infection. PLoS Pathog. 2019;15(1):1–14.
29. Gupta PK, Godec J, Wolski D, Adland E, Yates K, Pauken KE, et al. CD39 Expression Identifies Terminally Exhausted CD8+ T Cells. PLoS Pathog. 2015;11:1–22.
30. Jones RB, Ndhlovu LC, Barbour JD, Sheth PM, Jha AR, Long BR, et al. Tim-3 expression defines a novel population of dysfunctional T cells with highly elevated frequencies in progressive HIV-1 infection. J Exp Med. 2008;205:2763–79.
31. Teigler JE, Zalinskyy G, Eller MA, Bolton DL, Marovich M, Gordon AD, et al. Differential Inhibitory Receptor Expression on T Cells Delineates Functional

Capacities in Chronic Viral Infection. J Virol. 2017;91:e01263-17.
32. Tian X, Zhang A, Qiu C, Wang W, Yang Y, Qiu C, et al. The Upregulation of LAG-3 on T Cells Defines a Subpopulation with Functional Exhaustion and Correlates with Disease Progression in HIV-Infected Subjects. J Immunol. 2015;194:3873–82.
33. Chen H, Moussa M, Catalfamo M. The Role of Immunomodulatory Receptors in the Pathogenesis of HIV Infection: A Therapeutic Opportunity for HIV Cure? Front Immunol. 2020;11:1–20.
34. Blanch-Lombarte O, Gálvez C, Revollo B, Jiménez-Moyano E, Llibre JM, Manzano JL, et al. Enhancement of Antiviral CD8+ T-Cell Responses and Complete Remission of Metastatic Melanoma in an HIV-1-Infected Subject Treated with Pembrolizumab. J Clin Med. 2019;8:2089.
35. Sakuishi K, Apetoh L, Sullivan JM, Blazar BR, Kuchroo VK, Anderson AC. Targeting Tim-3 and PD-1 pathways to reverse T cell exhaustion and restore anti-tumor immunity. J Exp Med. 2010;207:2187–94.
36. Harjunpää H, Guillerey C. TIGIT as an emerging immune checkpoint. Clin Exp Immunol. 2020;200(2):108–19.
37. Maruhashi T, Sugiura D, Okazaki IM, Okazaki T. LAG-3: from molecular functions to clinical applications. J Immunother cancer. 2020;8:e001014.
38. Attanasio J, Wherry EJ. HHS Public Access. 2017;44(5):1052–68.
39. Chiu CY, Chang JJ, Dantanarayana AI, Solomon A, Evans VA, Pascoe R, et al. Combination Immune Checkpoint Blockade Enhances IL-2 and CD107a Production from HIV-Specific T Cells Ex Vivo in People Living with HIV on Antiretroviral Therapy. J Immunol. 2022;208:54–62.
40. Vaddepally RK, Kharel P, Pandey R, Garje R, Chandra AB. Review of indications of FDA-approved immune checkpoint inhibitors per NCCN guidelines with the level of evidence. Cancers (Basel). 2020;12:1–19.
41. Twomey JD, Zhang B. Cancer Immunotherapy Update: FDA-Approved Checkpoint Inhibitors and Companion Diagnostics. AAPS J. 2021;23:1–11.
42. Gonzalez-Cao M, Morán T, Dalmau J, Garcia-Corbacho J, Bracht JWP, Bernabe R, et al. Assessment of the Feasibility and Safety of Durvalumab for Treatment of Solid Tumors in Patients with HIV-1 Infection: The Phase 2 DURVAST Study. JAMA Oncol. 2020;6:1063–7.
43. Fromentin R, DaFonseca S, Costiniuk CT, El-Far M, Procopio FA, Hecht FM, et al. PD-1 blockade potentiates HIV latency reversal ex vivo in CD4+ T cells from ART-suppressed individuals. Nat Commun. 2019;10:1–7.
44. Le Garff G, Samrib A, Lambert-Niclot S, Even S, Lavole A, Cadranel J, et al. Transient HIV-specific T cells increase and inflammation in an HIV-infected patient treated with nivolumab. Aids. 2017;31:1047–8.
45. Gay CL, Bosch RJ, Ritz J, Hataye JM, Aga E, Tressler RL, et al. Clinical trial of the anti-PD-L1 antibody BMS-936559 in HIV-1 infected participants on suppressive antiretroviral therapy. J Infect Dis. 2017;215:1725–33.
46. Guihot A, Marcelin AG, Massiani MA, Samri A, Soulié C, Autran B, et al. Drastic decrease of the HIV reservoir in a patient treated with nivolumab for lung cancer. Ann Oncol. 2017;29:517–8.
47. Uldrick TS, Adams S V., Fromentin R, Roche M, Fling SP, Gonçalves PH, et al. Pembrolizumab induces HIV latency reversal in people living with HIV and cancer on antiretroviral therapy. Sci Transl Med. 2022;14.
48. Deeks SG, Archin N, Cannon P, Collins S, Jones RB, de Jong MAWP, et al. Research priorities for an HIV cure: International AIDS Society Global Scientific

Strategy 2021. Nat Med. 2021;27:2085–98.
49. Chauvin JM, Pagliano O, Fourcade J, Sun Z, Wang H, Sander C, et al. TIGIT and PD-1 impair tumor antigen-specific CD8+ T cells in melanoma patients. J Clin Invest. 2015;125(5):2046–58.
50. Anderson AC, Joller N, Kuchroo VK. Lag-3, Tim-3, and TIGIT: Co-inhibitory Receptors with Specialized Functions in Immune Regulation. Immunity. 2016;44:989–1004.
51. Joller N, Kuchroo VK. Tim-3, Lag-3, and TIGIT. Curr Top Microbiol Immunol. 2017;410:127–56.
52. Schildberg FA, Klein SR, Freeman GJ, Sharpe AH. Coinhibitory Pathways in the B7-CD28 Ligand-Receptor Family. Immunity. 2016;44:955–72.
53. Noyan K, Nguyen S, Betts MR, Sönnerborg A, Buggert M. Human immunodeficiency virus type-1 elite controllers maintain low co-expression of inhibitory receptors on CD4+ T cells. Front Immunol. 2018;9:1–11.
54. Avery L, Filderman J, Szymczak-Workman AL, Kane LP. Tim-3 co-stimulation promotes short-lived effector T cells, restricts memory precursors, and is dispensable for T cell exhaustion. PNAS. 2018;115:2455–60.
55. Yates KB, Tonnerre P, Martin GE, Gerdemann U, Al Abosy R, Comstock DE, et al. Epigenetic scars of CD8+ T cell exhaustion persist after cure of chronic infection in humans. Nat Immunol. 2021;22:1020–9.
56. Andrews LP, Yano H, Vignali DAA. Inhibitory receptors and ligands beyond PD-1, PD-L1 and CTLA-4: breakthroughs or backups. Nat Immunol. 2019;20:1425–34.
57. Sabatos-Peyton CA, Nevin J, Brock A, Venable JD, Tan DJ, Kassam N, et al. Blockade of Tim-3 binding to phosphatidylserine and CEACAM1 is a shared feature of anti-Tim-3 antibodies that have functional efficacy. Oncoimmunology. 2018;7:1–9.
58. Pende D, Castriconi R, Romagnani P, Spaggiari GM, Marcenaro S, Dondero A, et al. Expression of the DNAM-1 ligands, Nectin-2 (CD112) and poliovirus receptor (CD155), on dendritic cells: Relevance for natural killer-dendritic cell interaction. Blood. 2006;107:2030–6.
59. Maaten L van der. Visualizing Data using t-SNE. J Mach Learn Res. 2008;219:187–202.
60. Hyunghoon Cho BB and JP. Generalizable and Scalable Visualization of Single-Cell Data Using Neural Networks. Cell Syst. 2018;7(2):185–91.
61. Core Team R development. R: a Language and Environment for Statistical Computing. Vol. 2, http://www.R-project.org/. 2008. 1–2630 p.
62. Roederer M, Nozzi JL, Nason MC. SPICE: Exploration and analysis of post-cytometric complex multivariate datasets. Cytom Part A. 2011;79 A:167–74.

Figure Legends

Figure 1. Patterns of IRs co-expression and correlations with CD4+ T -cell counts in PLWH. (A) Overview of study groups, healthy controls (HC), PLWH in early HIV-1-infection (Ei), and PLWH on fully suppressive ART in S1 and S2. **(B)** The expression of IRs summarized in the pie chart is none, one, two, or more than three IRs. For statistical analysis, we used permutation tests using SPICE software. **(C)** Scatter plots showing the median and interquartile ranges of IR combinations. **(D)** Scatter plots of $TIGIT^+$ expression alone in central memory (CM) and transitional memory (TM) CD8+ T cells and $TIGIT^+TIM\text{-}3^+$ frequencies in CM, effector memory (EM) and effector (EFF) CD8+ T cells. **(B-D)** IR combinations are color-coded as a gradient scale. Each subset is colored as indicated in the legend. Naïve CD8+ T cells are not shown. We used the Mann-Whitney test in unpaired samples and the Wilcoxon test in paired samples for statistical analysis. P-values: *<0.05, **<0.005 and ***<0.0005. **(E-G)** Correlations between CD4+ T-cell counts as a function of $TIGIT^+$, $TIGIT^+TIM\text{-}3^+$ and combinations of IRs from total CD8+ T cells and subsets in Ei (**E**), S1 (**F**), and S2 (**G**). Asterisks mark statistically significant values. All possible correlations of the 32 boolean IRs combinations are not shown. P-values: *<0.05, **<0.005 and ***<0.0005.

Figure 2. Unsupervised net-SNE and cellular clustering of total CD8+ T cells. (A) Gating strategy for the selection of total CD8+ T cells and concatenation of 1,988,936 events between HC (green), Ei (orange), S1 (light blue), and S2 (dark blue) groups. Merged groups are shown in black. **(B)** Representative net-SNE visualization of surface markers. The color gradient displays the relative marker expression. **(C)** Unsupervised KNN algorithm of 38 clusters colored according to the legend. Only clusters with statistical differences are represented in the legend. **(D)** Heatmap of the

median biexponential-transformed marker expression normalized to a -3 to 3 range of respective markers. Asterisks represent the clusters with statistical differences to HC (HC vs. Ei, S1, and S2; $p<0.05$). **(E)** Scatter plots showing the median and interquartile ranges of cell frequency to HC and PLWH on ART (HC vs. S1 or S2; $p<0.05$). Clusters with high similitudes (#5, #6, and #7), (#9 and #10), and (#12, #13, and #14) were merged to increase the number of cells in the quantitative assessments. We used the Mann-Whitney test in unpaired samples and the Wilcoxon test in paired samples for statistical analysis. P-values: =0.05, *<0.05, **<0.005, and ***<0.0005.

Figure 3. Unsupervised net-SNE and cellular clustering of polyclonal TCR-activated CD8+ T cells. (A) Gating strategy for the selection of polyclonal TCR-activated CD8+ T cells and concatenation of 253,021 events between HC (green), Ei (orange), S1 (light blue), and S2 (dark blue). Merged groups are shown in black. **(B)** Representative net-SNE visualization of IR expression, lineage, and functional markers. The color gradient displays relative marker expression. **(C)** Unsupervised KNN algorithm for 29 polyclonal clusters color-coded according to the legend. Clusters with statistical differences between groups are represented in the legend. **(D)** Heatmap of the median biexponential-transformed marker expression normalized to a -3 to 3 range of respective markers. Asterisks represent the clusters with statistical differences to HC (HC vs. Ei, S1, and S2; $p<0.05$). **(E)** Scatter plots showing the median and interquartile ranges of polyclonal TCR-activation frequency in HC to PLWH on ART (HC vs. S1 or S2; $p<0.05$). Clusters with high similitudes (#1 and #2), (#4 and #5), and (#8, #9, and #10) were merged to increase the number of polyclonal cells in the quantitative assessments. We used the Mann-Whitney test in unpaired samples and the Wilcoxon

test in paired samples for statistical analysis. P-values: *<0.05, **<0.005, and ***<0.0005.

Figure 4. Unsupervised single-cell analyses and supervised classical gating of HIV-1-specific CD8+ T cells. (A) Selection of HIV-1-specific CD8+ T cells producing at least CD107a, IFNγ, or IL-2 and concatenation for Ei (orange), S1 (light blue), and S2 (dark blue). 53,751 events for HIV-1-specific CD8+ T cells were acquired and merged between the groups (black). **(B)** Different net-SNE plots with the expression of surface and functional markers. The color gradient displays the relative expression. **(C)** Unsupervised KNN algorithm for 26 HIV-1-specific clusters color-coded according to the legend. Only clusters with statistical differences are represented in the legend. **(D)** Heatmap of the median biexponential-transformed marker expression normalized to a -3 to 3 range of respective markers. Asterisks represent the clusters with statistical differences to PLWH in early HIV-1-infection (Ei vs. S1 and S2; p<0.05). **(E)** Scatter plots showing the median and interquartile ranges of HIV-1-specific CD8+ T cells. **(F)** Pie chart forms (left panel) representing the combinations from one, two, or three functional markers. We used permutation tests in pie chart forms for statistical analysis between groups. Scatter plots (central panel) showing the median and interquartile ranges of one, two, or three functional combinations. Scatter plots (right panel) the median and interquartile representing ranges for single combination of $CD107a^+$ (purple), $IFN\gamma^+$ (red), and $IL\text{-}2^+$ (pink) from HIV-1-specific CM CD8+ T cells expressing $TIGIT^+$ alone. We used the Mann-Whitney test in unpaired samples and the Wilcoxon test in paired samples for statistical analysis. P-values: =0.05, *<0.05, **<0.005, ***<0.0005, and ****<0.0001.

Figure 5. **TIGIT but not TIGIT+TIM-3 pathway blockade restores CD107a expression in HIV-1-specific CD8+ T cells in PLWH on ART. (A)** Representative net-SNE flow cytometry projections with surface and functional markers. 65,445 acquired HIV-1-specific CD8+ T cells from PLWH on fully suppressive ART (S1 and S2) were concatenated and merged according to the condition; HIV-1 stimulation (red), HIV-1 with isotype (grey), HIV-1 with αTIGIT (blue), and HIV-1 with αTIGIT+αTIM-3 (green). αTIGIT and its respective isotype are merged as histograms to highlight differences between conditions. **(B)** Scatter plots showing the median and interquartile ranges of the frequency of CD107a in total HIV-1-specific CD8+ T cells after αTIGIT and αTIGIT+αTIM-3. **(C)** Frequency of CD107a in HIV-1-specific CD8+ T-cell subsets after αTIGIT and **(D)** after αTIGIT+αTIM-3. **(B-D)** Statistical differences were calculated by the Wilcoxon matched-pairs signed ranked test. P-values: =0.05, *<0.05, **<0.005 and ***<0.0005.

Supplemental Figures

Figure Supplemental 1. IRs profiling of CD8+ T-cells across study groups. (A) Flow cytometric gating strategy to analyze the frequency of TIGIT, PD-1, LAG-3, TIM-3, and CD39 in total and CD8+ T-cell subsets. **(B)** Scatter plots with the median and interquartile ranges of frequency in population and IR expression for total CD8+ T cells between healthy controls (HC), PLWH in early HIV-1-infection (Ei), and PLWH on fully suppressive ART in S1 and S2, and **(C)** for CD8+ T-cell subsets. Due the low expression of IRs on naïve, data are not shown. We used the Mann-Whitney test for unpaired samples and the Wilcoxon test for paired samples for statistical analysis. **(D)** Poly-expression patterns for the 32 possible combinations for TIGIT, PD-1, LAG-3, TIM-3, and CD39 in CD8+ T-cell subsets. Each pie chart form and arcs are color-coded according to the combinations of IRs. All scatter plots with the median and interquartile ranges of frequency of each population are not shown. We used permutation tests of SPICE software for statistical analysis. P-values: *<0.05, **<0.005, ***<0.0005, ****<0.00005.

Supplemental Table 1. Epidemiological characteristics of the study groups.

Study Groups	Healthy Control	Early HIV-1 infection	HIV-1 on ART		
	HC	Ei	S1	S2	
Number of subjects	24	24	24	24	
Age (years) [median (IQR)]	43.1 (38.1 - 52.5)	43.3 (41.8 - 46.2)	40.6 (35.1 - 44.7)	50.0 (43.7 - 55.1)	0.059
Gender (M/F) [n (%)]	16/8 (67/33%)	23/1 (96/4%)	18/6 (75/25%)	18/6 (75/25%)	0.091
CD4+ T-cell counts per mm^3 [median (IQR)]	-	630 (557 - 757.3)	573 (464 - 992)	910 (799.8 - 1111	**0.0001**
Weeks since seroconversion [median (IQR)]	-	1.3 (0.77 - 17.8)	-	-	
Years undetectable on ART [median (IQR)]	-	0.0	2.2 (1.8 - 2.8)	10.1 (7.4 - 12.9)	**<0.0001**
VL log copies/ml [median (IQR)]	-	4.5 (4.3 - 5.1)	undetectable	undetectable	**<0.0001**

Abbreviations: IQR, interquartile range; P-values were calculated using Kruskal-Wallis test (Dunn´s correction) or X^2-test.

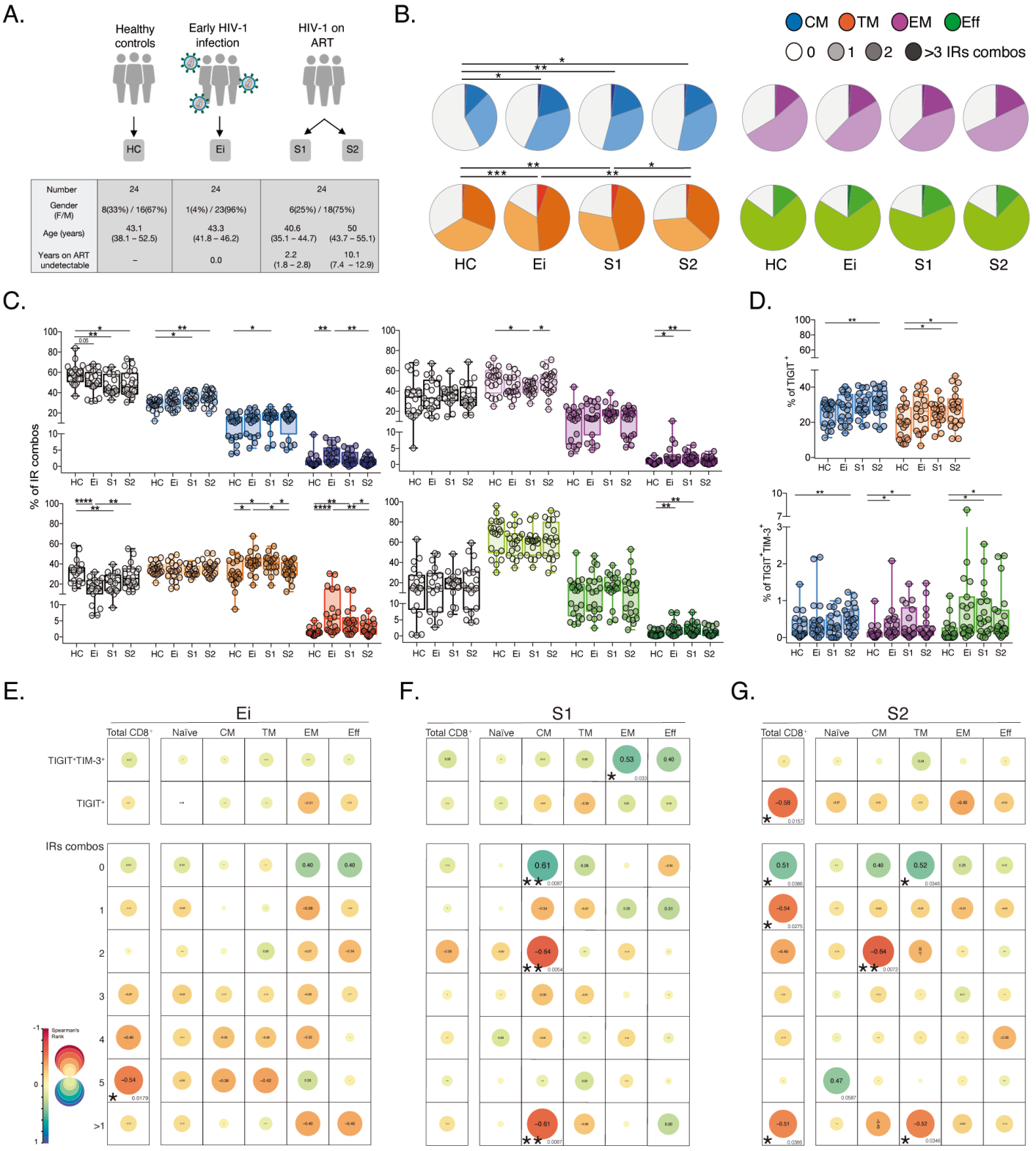

Figure 1. Patterns of IRs co-expression and correlations with CD4+ T -cell counts in PLWH. (A) Overview of study groups, healthy controls (HC), PLWH in early HIV-1-infection (Ei), and PLWH on fully suppressive ART in S1 and S2. (B) The expression of IRs summarized in the pie chart is none, one, two, or more than three IRs. For statistical analysis, we used permutation tests using SPICE software. (C) Scatter plots showing the median and interquartile ranges of IR combinations. (D) Scatter plots of TIGIT+ expression alone in central memory (CM) and transitional memory (TM) CD8+ T cells and TIGIT+TIM-3+ frequencies in CM, effector memory (EM) and effector (EFF) CD8+ T cells. (B-D) IR combinations are color-coded as a gradient scale. Each subset is colored as indicated in the legend. Naïve CD8+ T cells are not shown. We used the Mann-Whitney test in unpaired samples and the Wilcoxon test in paired samples for statistical analysis. P-values: *<0.05, **<0.005 and ***<0.0005. (E-G) Correlations between CD4+ T-cell counts as a function of TIGIT+, TIGIT+TIM-3+ and combinations of IRs from total CD8+ T cells and subsets in Ei (E), S1 (F), and S2 (G). Asterisks mark statistically significant values. All possible correlations of the 32 boolean IRs combinations are not shown. P-values: *<0.05, **<0.005 and ***<0.0005.

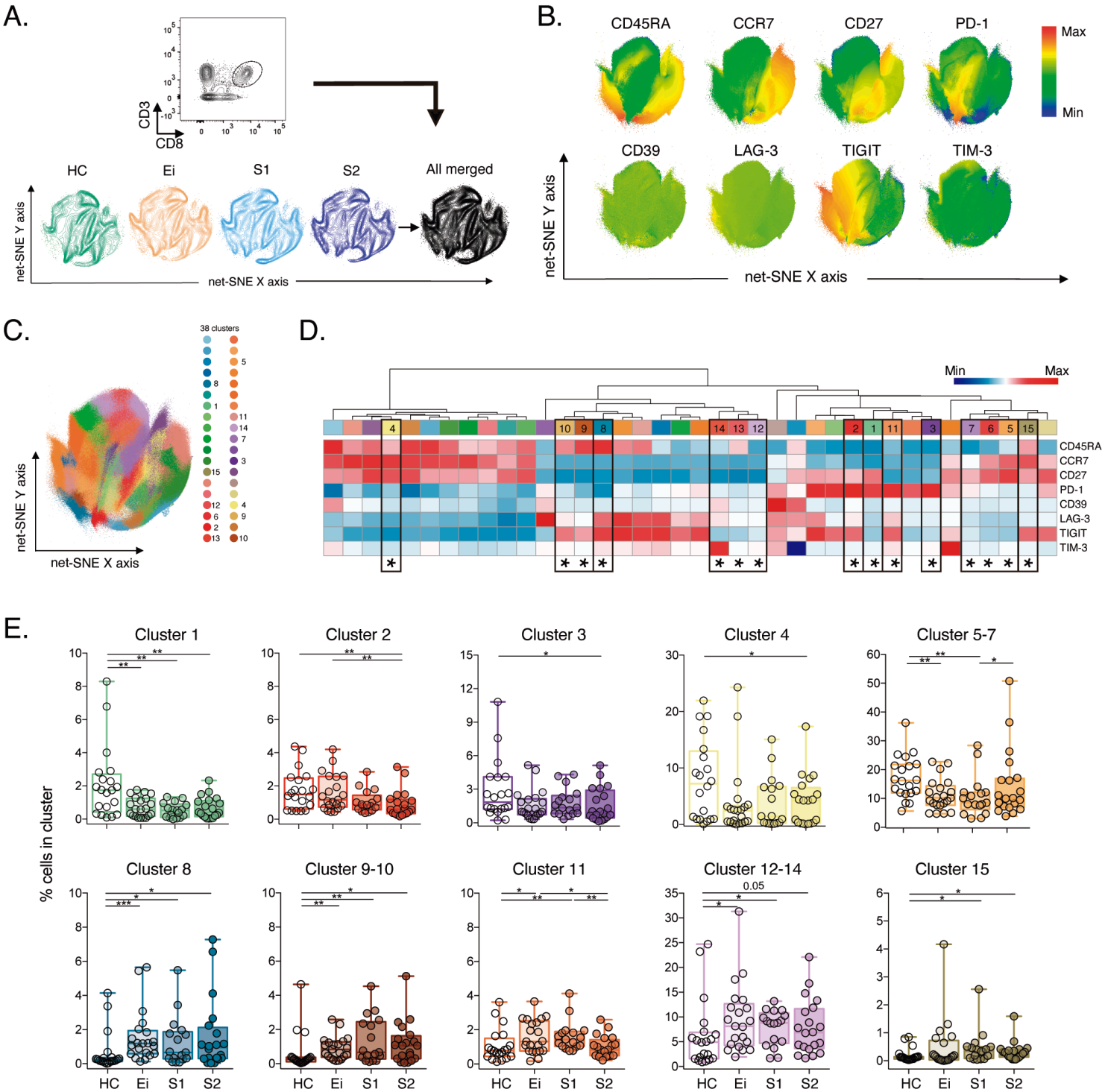

Figure 2. Unsupervised net-SNE and cellular clustering of total CD8+ T cells. (A) Gating strategy for the selection of total CD8+ T cells and concatenation of 1,988,936 events between HC (green), Ei (orange), S1 (light blue), and S2 (dark blue) groups. Merged groups are shown in black. (B) Representative net-SNE visualization of surface markers. The color gradient displays the relative marker expression. (C) Unsupervised KNN algorithm of 38 clusters colored according to the legend. Only clusters with statistical differences are represented in the legend. (D) Heatmap of the median biexponential-transformed marker expression normalized to a -3 to 3 range of respective markers. Asterisks represent the clusters with statistical differences to HC (HC vs. Ei, S1, and S2; $p<0.05$). (E) Scatter plots showing the median and interquartile ranges of cell frequency to HC and PLWH on ART (HC vs. S1 or S2; $p<0.05$). Clusters with high similitudes (#5, #6, and #7), (#9 and #10), and (#12, #13, and #14) were merged to increase the number of cells in the quantitative assessments. We used the Mann-Whitney test in unpaired samples and the Wilcoxon test in paired samples for statistical analysis. P-values: =0.05, *<0.05, **<0.005, and ***<0.0005.

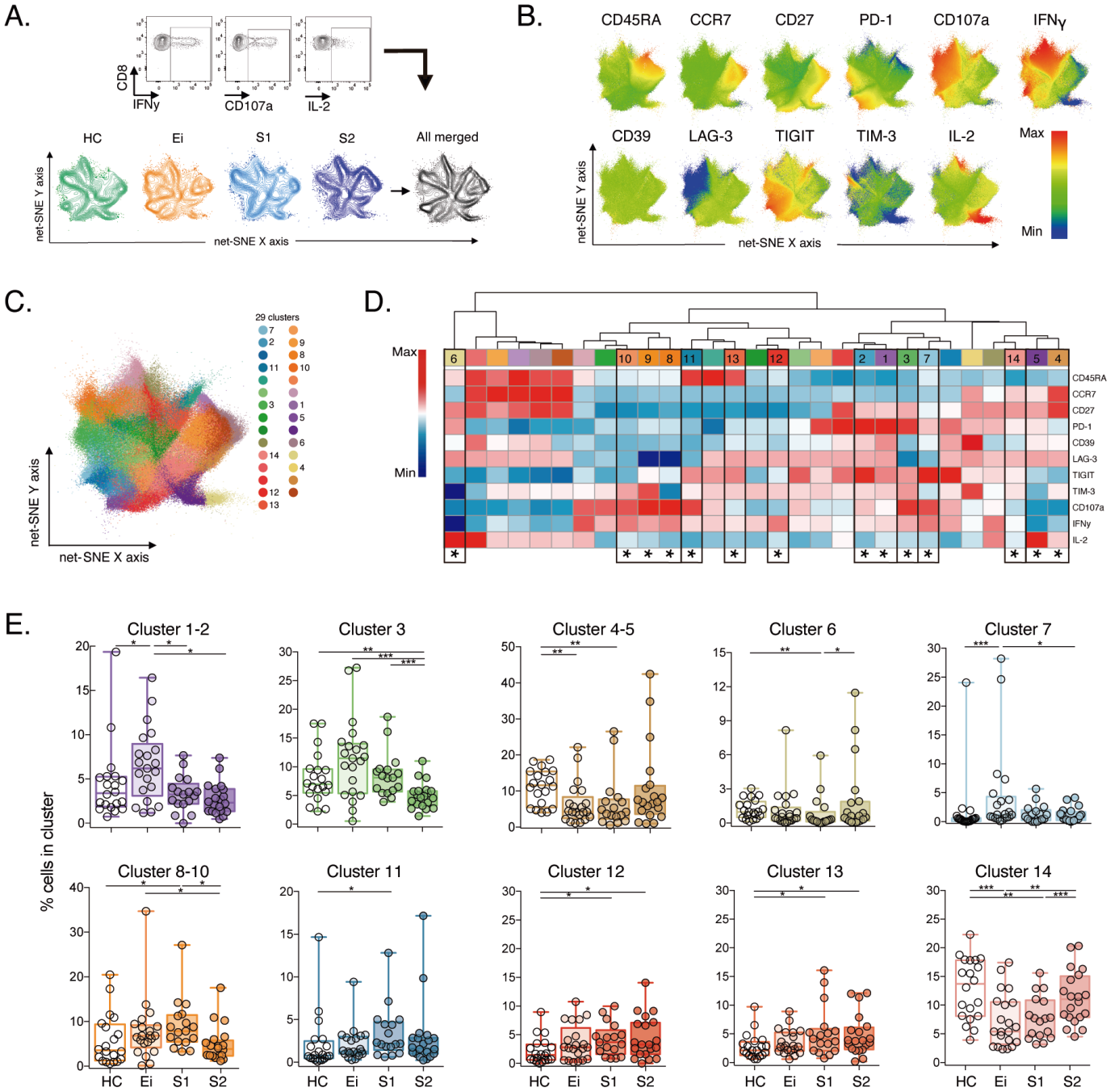

Figure 3. Unsupervised net-SNE and cellular clustering of polyclonal TCR-activated CD8+ T cells. (A) Gating strategy for the selection of polyclonal TCR-activated CD8+ T cells and concatenation of 253,021 events between HC (green), Ei (orange), S1 (light blue), and S2 (dark blue). Merged groups are shown in black. (B) Representative net-SNE visualization of IR expression, lineage, and functional markers. The color gradient displays relative marker expression. (C) Unsupervised KNN algorithm for 29 polyclonal clusters color-coded according to the legend. Clusters with statistical differences between groups are represented in the legend. (D) Heatmap of the median biexponential-transformed marker expression normalized to a -3 to 3 range of respective markers. Asterisks represent the clusters with statistical differences to HC (HC vs. Ei, S1, and S2; $p<0.05$). (E) Scatter plots showing the median and interquartile ranges of polyclonal TCR-activation frequency in HC to PLWH on ART (HC vs. S1 or S2; $p<0.05$). Clusters with high similitudes (#1 and #2), (#4 and #5), and (#8, #9, and #10) were merged to increase the number of polyclonal cells in the quantitative assessments. We used the Mann-Whitney test in unpaired samples and the Wilcoxon test in paired samples for statistical analysis. P-values: *<0.05, **<0.005, and ***<0.0005.

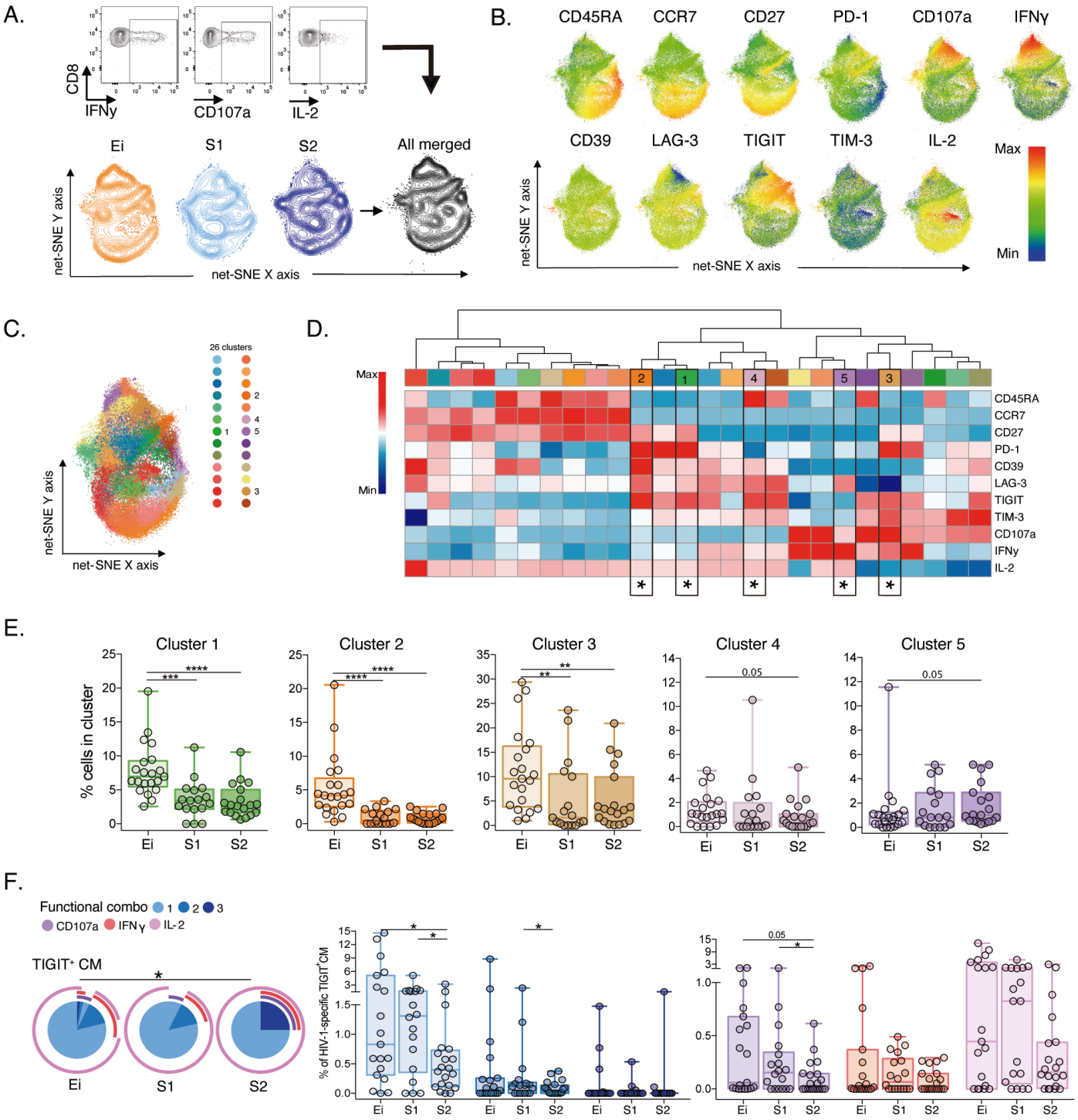

Figure 4. Unsupervised single-cell analyses and supervised classical gating of HIV-1-specific CD8+ T cells. (A) Selection of HIV-1-specific CD8+ T cells producing at least CD107a, IFNγ, or IL-2 and concatenation for Ei (orange), S1 (light blue), and S2 (dark blue). 53,751 events for HIV-1-specific CD8+ T cells were acquired and merged between the groups (black). (B) Different net-SNE plots with the expression of surface and functional markers. The color gradient displays the relative expression. (C) Unsupervised KNN algorithm for 26 HIV-1-specific clusters color-coded according to the legend. Only clusters with statistical differences are represented in the legend. (D) Heatmap of the median biexponential-transformed marker expression normalized to a -3 to 3 range of respective markers. Asterisks represent the clusters with statistical differences to PLWH in early HIV-1-infection (Ei vs. S1 and S2; p<0.05). (E) Scatter plots showing the median and interquartile ranges of HIV-1-specific CD8+ T cells. (F) Pie chart forms (left panel) representing the combinations from one, two, or three functional markers. We used permutation tests in pie chart forms for statistical analysis between groups. Scatter plots (central panel) showing the median and interquartile ranges of one, two, or three functional combinations. Scatter plots (right panel) the median and interquartile representing ranges for single combination of CD107a+ (purple), IFNγ+ (red), and IL-2+ (pink) from HIV-1-specific CM CD8+ T cells expressing TIGIT+ alone. We used the Mann-Whitney test in unpaired samples and the Wilcoxon test in paired samples for statistical analysis. P-values: =0.05, *<0.05, **<0.005, ***<0.0005, and ****<0.0001.

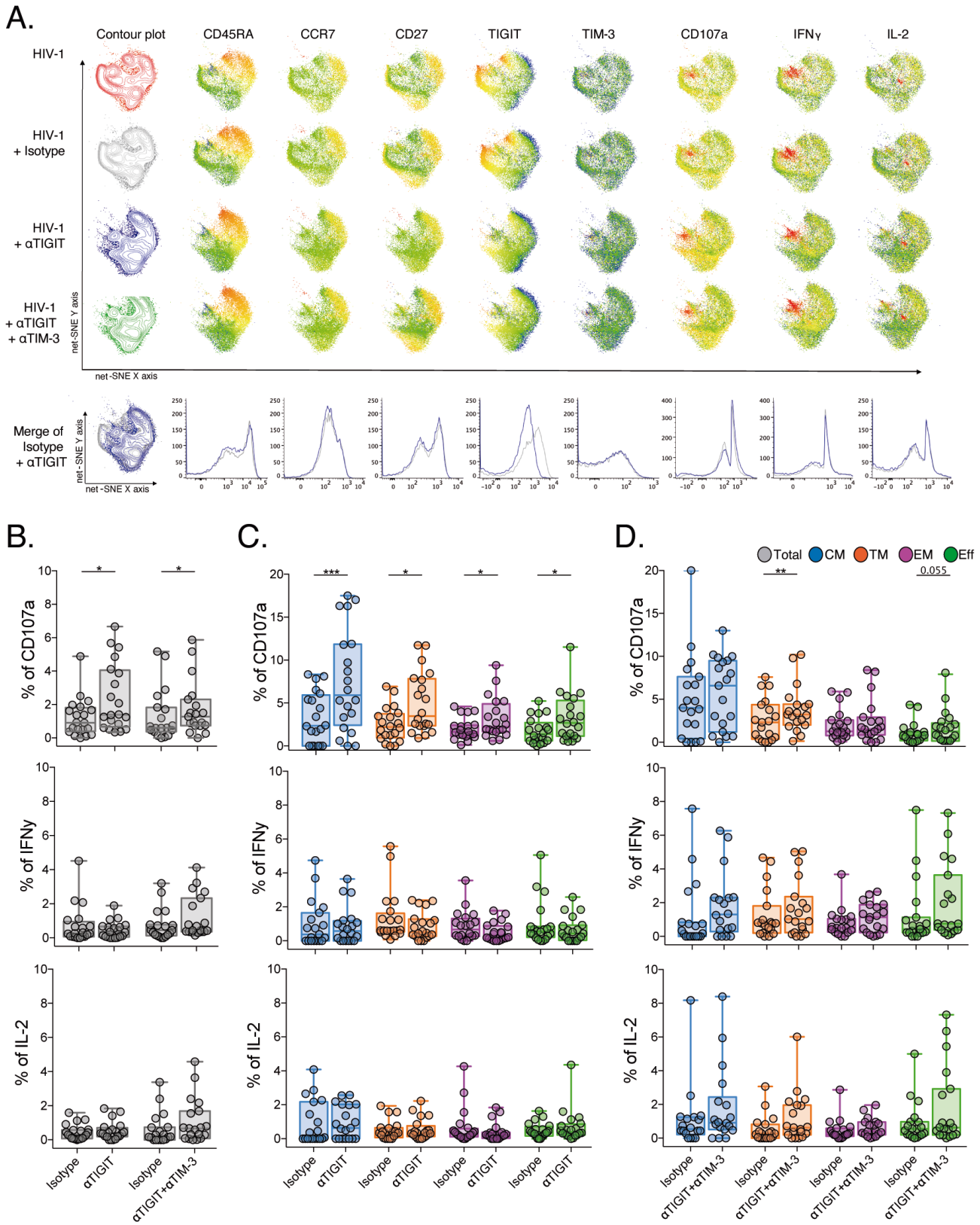

Figure 5. TIGIT but not TIGIT+TIM-3 pathway blockade restore CD107a expression in HIV-1-specific CD8+ T cells in PLWH on ART. (A) Representative net-SNE flow cytometry projections with surface and functional markers. 65,445 acquired HIV-1-specific CD8+ T cells from PLWH on fully suppressive ART (S1 and S2) were concatenated and merged according to the condition; HIV-1 stimulation (red), HIV-1 with isotype (grey), HIV-1 with α TIGIT (blue), and HIV-1 with αTIGIT+αTIM-3 (green). αTIGIT and its respective isotype are merged as histograms to highlight differences between conditions. (B) Scatter plots showing the median and interquartile ranges of the frequency of CD107a in total HIV-1-specific CD8+ T cells after αTIGIT and αTIGIT+αTIM-3. (C) Frequency of CD107a in HIV-1-specific CD8+ T-cell subsets after αTIGIT and (D) after αTIGIT+αTIM-3. (B-D) Statistical differences were calculated by the Wilcoxon matched-pairs signed ranked test. P-values: =0.05, *<0.05, **<0.005 and ***<0.0005.